M Beckers et al.

Investigations of the First-Wall Erosion of DEMO with the CELLSOR Code

Investigations of the First-Wall Erosion of DEMO with the CELLSOR Code

M. Beckers, W. Biel, M. Tokar, U. Samm

Forschungszentrum Jülich GmbH, Institut für Energie- und Klimaforschung - Plasmaphysik, 52425 Jülich, Germany

m.beckers@fz-juelich.de

Abstract

Fusion reactor systems codes (SCs) are 0.5d codes used for optimization studies towards the design of a tokamak demonstration power plant (DEMO). These codes usually comprise a description of the core plasma physics, technology aspects and reactor economy, while only a coarse description of plasma-wall interaction (PWI) aspects is included. Therefore, the new systems code extension CELLSOR (Code to Estimate the Lifetime Limited by Sputtering Of a Reactor wall) was developed in order to allow inclusion of PWI effects into reactor optimization studies. CELLSOR is foreseen to be used as a secondary tool for PWI evaluations, taking design point parameters from the European PROCESS systems code as input. CELLSOR consists of an analytical treatment of the plasma in the scrape-off layer (SOL) for fuel ions (D, T), solving the 1.5d continuity equation in fluid approximation to obtain perpendicular flux and ion density in the SOL, and a fast Monto-Carlo description of the neutral particle (D, T) behavior. The trajectories of neutral W are computed within CELLSOR ERO, an add-on code used for calculations of prompt redeposition and self-sputtering. Within the analytic description of ion damage, i.e. by fuel, ash (He), seeding gas (N, Ar, Kr) and wall material (W), impurity concentrations are assumed to be radially constant.

For the core plasma, pre-scribed radial profiles of density and temperature are used, including a parametric model of the pedestal profiles. The primary erosion of the tungsten first wall is calculated based on contributions by the plasma fluxes (fuel and impurity ions), including the acceleration by a sheath in front of the wall, as well as by energetic (> 1 keV) neutrals which are mainly originating from charge exchange (CX) collisions of the recycled neutrals from the wall re-entering the hot pedestal region. In this description, the primary erosion of the first wall depends on the radial transport coefficients (diffusivity, convection), the parallel time of transport to the divertor, the gap between separatrix and first wall and the plasma parameters in the pedestal (temperature at the top / separatrix).

The Monte Carlo (MC) implementation of the new code extension has been successfully benchmarked with results from the EIRENE code. CELLSOR calculations with medium transport ($D_\perp = 0.5\ \mathrm{m^2s^{-1}}$, $v_\perp = 5\ \mathrm{ms^{-1}}$, reference case) showed for the net mass erosion by ions and neutrals, that the gap parameter needs to be at least $\Delta_{SOL} > 0.08$ m to achieve component lifetimes > 1 fpy (minimum feasibility criterion). The results of PWI studies indicate, that lower densities at the upper midplane are favorable for DEMO operation. However, the upstream density has to be sufficiently high for divertor detachment and fusion performance. The gap parameter showed a strong flux effect within diffusive SOL transport regimes, being suppressed in the convective density shoulder case, where a very strong transport was assumed. Nevertheless, the controllability of the SOL transport regime remains unclear for DEMO. Of course, the gap size effect increases rapidly for weak transport and decreases slightly for strong transport. Furthermore, the sputter yield of impinging CX neutrals was changing within a factor of $1.7 - 1.8$, for variations of the pedestal top temperature between 4 and 8 keV.

1. Introduction

ITER is currently being built in Cardarache in France to proof the technological viability of tokamaks as a milestone towards a fusion power plant (*FPP*) [1, 2]. Meanwhile, a European *DEMO* is being developed and foreseen to be operated by the year 2050 [3]. In order to identify feasible parameter ranges for DEMO, fast reactor SCs are used in the early design phase [3]. PROCESS [4] and SYCOMORE [5] are currently the main tools of the European DEMO program.

For *DEMO*, several wall concepts are being discussed, sharing the main material *W* on the plasma-facing side of the first-wall (*FW*). During tokamak operation, *W* is eroded by sputtering by plasma ions, including fuel (*D*, *T*), ash (He), seeding gas (*N, Ne, Ar, Kr, Xe*) and eroded wall material (*Fe, W*). Close to the wall, ions are accelerated inside the Debye Sheath to energies that may exceed the sputter threshold. Further damage is made by neutral particles, mainly energetic *D* and *T* atoms, which are released from hot plasma regions by CX between cold, recycled neutrals, and hot plasma ions [6].

Sputter damage may be further amplified by self-sputtering, i.e. $W^+ \rightarrow W$ [7] or repaired by prompt redeposition of eroded material, occurring when the ionization length for $W \rightarrow W^+$ is within the gyro-radius of W^+ [7, 8].

In order to incorporate FW erosion into SC studies, CELLSOR was written as a fast and flexible extension, creating a linkage between plasma parameters and *FW* erosion. The heart of *CELLSOR* is a *1.5d MC* code, which allows calculations of the sputtering by *D* and *T* neutrals. The add-on MC code CELLSOR ERO allows additional estimations of self-sputtering and prompt redeposition, assuming Thompson distributions for the velocities of eroded material and $\cos(\theta)$ angular distribution. Sputter contributions by ions are estimated assuming impurity concentrations and charge states at the entrance of the Debye Sheath. The consistent perpendicular wall influx and the SOL ion density profile are obtained by analytical solutions of a 1.5d continuity equation, using the neutral density profiles obtained by CELLSOR creating the volumetric source term.

Within this work, the wall damage, i.e. global average net erosion calculated from sputter yields of ions and neutrals, are investigated for different plasma parameters, within the pedestal and scrape-off layer region. Variations were conducted to the SOL width Δ_{SOL}, the transport strengths $D_\perp$ (diffusive) and $v_\perp$ (convective), and pedestal and separatrix values for electron density and temperature.

2. Methods

Within this section, the methods to estimate the damage by neutrals and ions are described. The main part is the MC code CELLSOR, which focuses on the neutral damage, which can be comparable to the ion damage on DEMO-like machines. However, rudimentary estimates for ion damage are also included for a complete analysis of the net erosion.

2.1. The Monte Carlo Code CELLSOR

The *1.5d* code *CELLSOR* was written in *python2.7*, *cython* and *numerical python*. CELLSOR solves kinetic equations within a torus in a *3d* algebraic space (steadiness of kinetic equations, angle dependency of sputter yields), because of the angle-dependency of the sputter yield $Y(\theta, E)$. Therefore, the torus was divided into cell boundary surfaces, i.e. centered – but smaller - torus surfaces of radii $\rho_{cellbound}$. Cells represent the space between cell boundary surfaces, being centered at radial positions ρ_{cell} with a width of Δ_{cell}. The outermost torus surface at $\rho_{wall} = a + \Delta_{SOL}$ describes the main chamber *FW* position. Cells were equidistantly distributed between the plasma centre and the wall position.

2.1.1. Plasma Profiles

The concept of test-particle *MC* comprises linear independency between simulated particles, which is granted by the simulation of the interaction of a neutral particle with a stationary plasma background. The background is given by 1d radial profiles, i.e. volume-averaged electron temperature and line-averaged – density, divided into a plasma core (parabolic), plasma edge (linear), and a *SOL* (exponential) region. Accordingly, the temperature profile was computed

(1) $\langle T \rangle(r) =$
$$\begin{cases} \langle T \rangle_{ped} + (\langle T \rangle_0 - \langle T \rangle_{ped})\left(1 - \left(\frac{r}{r_{ped}}\right)^2\right)^{\alpha_T} & \text{,if } r \le r_{ped} \\ mr + b & \text{,if } r_{ped} < r \le a \\ \langle T \rangle_{sep} e^{\left(\frac{-(r-a)}{\lambda_t}\right)} & \text{,otherwise} \end{cases}$$

with $m = \frac{\langle T \rangle_{sep} - \langle T \rangle_{ped}}{\Delta_{ped}}$, $b = \langle T \rangle_{sep} - ma$. The density profile $\bar{n}(r)$ was constructed similarly, however, in "consistency mode", the SOL part of the profile was calculated from particle balance, i.e. instead of a decay parameter λ_n, the profile is constructed from the transport parameters $D_\perp$ and $v_\perp$ and the volumetric source strength S (section 2.2).

2.1.2. Physical Reactions

Reaction rate coefficients are used for simulation of the interaction of test-particles with the plasma background. Within each cell, the physical reaction probability

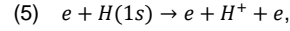(2) $p = 1 - e^{((-t_{dwell}\langle \sigma v \rangle))}$

is determined by the dwell time inside the cell and the reaction rate coefficients, which were taken from [9] and [10] for molecular dissociation and -ionization, and atomic CX and -ionization. Included reactions are molecular dissociation
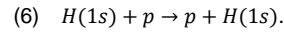
(3) $e + H_2 \rightarrow e + H(1s) + H(1s)$,
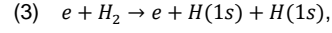
molecular ionization

(4) $e + H_2 \rightarrow e + H_2^+ + e$,
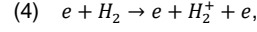
atomic ionization of hydrogen by an electron

(5) $e + H(1s) \rightarrow e + H^+ + e$,

and CX between an hydrogen atom and a plasma background ion

(6) $H(1s) + p \rightarrow p + H(1s)$.

2.1.3. Sputter Yields

Sputter yields are affected by the angle of incidence and the energy of projectile particles, derived from the velocity vectors of test-particles inside the torus. They provide information about the relative number of eroded surface atoms per impinging projectile particle. For neutral *D-/T-* atoms, sputter yields are interpolated, using experimental data (energy-angle tables) from [11]. Their kinetic energy is given by $E_{kin} = 0.5m|\vec{v}|^2$ and their angle of incidence is calculated algebraically from the wall surfacenormal- and the velocity vectors.

2.2. Particle Balance

Within the SOL region, the profiles satisfy particle balance, i.e. balance between perpendicular flux onto the wall and parallel flux into the divertor, taking into account volumetric effects. In "consistency mode", flux balance is calculated with a continuity equation, using the neutral density profile calculated by *MC* for volumetric source construction. In "explorer mode", the SOL density profile is pre-defined by an exponentially decaying function with the decay parameter λ_n.

2.2.1. Continuity Equation

In "consistency mode", the ion density profile is derived from a stationary continuity equation, formulated in carthesian coordinates for analytical treatment (eq. 7).

(7) $\frac{d}{dx}\left(-D_\perp \frac{d\bar{n}_i}{dx} + \bar{n}_i v_\perp\right) = -\frac{\bar{n}_i}{\tau_{loss}} + S$

The source S is obtained from MC (1d) and $D_\perp, v_\perp$ and τ_{loss} are input parameters (0d). The particle loss time to the divertor was estimated at the upper midplane position as $\tau_{loss} \approx \frac{L_\parallel}{v_\parallel} \approx \frac{90 \text{ m}}{1.8 \cdot 10^4 \text{ m/s}} = 5$ms. For derivation of an analytic ion density solution function, boundary conditions at the separatrix- ($x = 0$: $\bar{n}_i = \bar{n}_{i,sep}$) and wall-position ($x = \Delta_{SOL}$: $\nabla\bar{n}_i = -\bar{n}_i/\delta$) were defined. The boundary parameter δ is in the order of the ion larmor radius, i.e. $\delta \approx 3e^{-4}$, being the minimum decay length due to perpendicular transport (similar treatment in [12]).

After substitutions of the transport parameters, and the source term S into $Q(x) = \langle \sigma v_x \rangle_{iz} \bar{n}_i \bar{n}_n'$ (eq. 8-12), which

scales with the recycling factor R_{rec} instead of the unknown ion influx $\Gamma_\perp$ ($\bar{n}_n'$ was taken directly from *MC*), the ion density is expressed by an analytic expression (eq. 13).

(8) $\lambda_1 = g + \sqrt{g^2 + q}, \quad \lambda_2 = p - \sqrt{g^2 + q},$

(9) $\Psi_1(x) = \eta \int_x^{\Delta_{SOL}} Q(y) \exp[\lambda_1(x-y)]dy,$

(10) $\Psi_2(x) = \eta \int_0^x Q(y) \exp[\lambda_2(x-y)]dy,$

(11) $\eta = 1 + \frac{\lambda_2}{\frac{1}{\delta} + \lambda_2},$

(12) $\kappa = 1 + \frac{\lambda_2 - \lambda_1}{\frac{1}{\delta} + \lambda_1}.$

(13) $\bar{n}_i(x) =$
$\bar{n}_{i,sep} \frac{\exp(\lambda_2 x) - \kappa \exp[\lambda_2 \Delta_{SOL} - \lambda_1(\Delta_{SOL} - x)]}{1 - \kappa \exp[(\lambda_2 - \lambda_1)\Delta_{SOL}] + \Psi_1(0)\exp(\lambda_2 \Delta_{SOL}) - \Psi_2(\Delta_{SOL})} +$
$\bar{n}_{i,sep} \frac{[\Psi_1(x) + \Psi_2(x)]\exp(\lambda_2 \Delta_{SOL}) - \Psi_2(\Delta_{SOL})\exp(\lambda_2 x)}{1 - \kappa \exp[(\lambda_2 - \lambda_1)\Delta_{SOL}] + \Psi_1(0)\exp(\lambda_2 \Delta_{SOL}) - \Psi_2(\Delta_{SOL})}$

2.2.2. Iterations

Due to the non-linear feedback between $\bar{n}_i(x)$ and $\bar{n}_n'(x)$, iterations between kinetic- (CELLSOR) and fluid calculations (continuity equation) are necessary to obtain solutions obeying the particle balance. For smoothing, the source term $Q(x)$ is subsequently switched on with a mixing factor $0 \leq A_{mix} \leq 1$.

(14) $\bar{n}_n^0(x) = 0 \quad \rightarrow \quad Q_0 = 0 \quad \rightarrow \quad \Psi_{1,2}^0(x) = 0$

(15) $\bar{n}_i^0(x) = \bar{n}_{i,sep} \frac{\exp(\lambda_2 x) - \kappa \exp[\lambda_2 \Delta_{Sol} - \lambda_1(\Delta_{Sol} - x)]}{1 - \kappa \exp[(\lambda_2 - \lambda_1)\Delta_{Sol}]}$

The solution procedure starts with a 0-approximation solution, i.e. without volumetric source (eq. 14-15).

(16) $Q_l(x) = (1 - A_{mix})Q_{l-1}(x) + A_{mix}\langle\sigma v\rangle_{iz}\bar{n}_i^{l-1}(x)\bar{n}_n^l(x)$

$$\rightarrow \quad \Psi_{1,2}^l(x) \quad \rightarrow \quad \bar{n}_i^l(x)$$

In the following *l*-approximation solution, the neutral density $n_n^l(x)$ from *MC*, yielding Q_l as in eq. 16, is used to calculate the ion density profile of $n_i^{l-1}(x)$ as in eq. 13. A comparably small change of the ion density at the FW, i.e. $\nabla\bar{n}_i(\Delta_{SOL}) \ll A_{mix}$, is used as convergence criterion, with $A_{mix} = 1$ at convergence.

2.2.3. Particle Flux Density

Equations 7-16 showed the recipe to obtain an analytic ion density profile in the *SOL*, that is consistent with the transport and the neutral density profile, calculated by *MC*. The perpendicular ion flux onto the FW is

(17) $\Gamma_\perp = -D_\perp \nabla\bar{n}_i + \bar{n}_i v_\perp.$

2.3. The add-on code CELLSOR ERO

The CELLSOR code provides information about the sputter yield by D-/T neutral projectiles. The consistent ion density profile, together with the information about neutral particle sputter yields and recycling flux, are transferred as input values to a secondary and similar MC code, named CELLSOR ERO, which traces eroded W atoms instead of D- and T neutrals. The purpose of CELLSOR ERO is to estimate prompt redeposition of eroded W as well as self-sputtering.

2.3.1. Probability density function of eroded W

A broadly used approach for description of eroded particles, is a Thompsonian energy distribution [13], with a cutoff related to the energy of the eroding projectile species, together with a $\cos(\theta)$ angular distribution. The effective sputter yields of different ion species and the hydrogen neutrals computed with CELLSOR, define the probabilities for each Thompsonian, whose probability density function (pdf) is given by eq. 18.

(18) $p_{thomp}(E) = A \frac{E}{(E + E_{sb})^3}$

2.3.2 Plasma-Particle Reaction

Within CELLSOR ERO, the ionization of a neutral W test-particle with the plasma background (eq. 19, rate coefficient from [14]) is considered

(19) $e + W \rightarrow e + W^+ + e.$
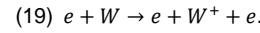
2.3.3. Prompt Redeposition

The prompt redeposition is estimated as in [8] for each simulated test-particle i of an ensemble N by comparison of the ionization distance to the wall λ_{ion} and the larmor-radius ρ_{gyro} as in eq. 20-21, and finally being averaged over all simulated test-particles (eq. 22).

(20) $p_i = \frac{\lambda_{ion,i}}{\rho_{gyro,i}}$

(21) $f_{dep,i} = 0.5 \cdot \left(1 + sig(1 - p_i)\left\{\frac{(1 + 4p_i^2)}{(1 - p_i^2)^2}\right\}^{-0.5}\right)$

(22) $f_{dep} = \frac{\sum_i f_{dep,i}}{N}$

2.3.4. Ion Damage

Ions are especially harmful to the FW, because – other than neutrals - they are accelerated by the sheath potential (eq. 23, see [15]).

(23) $V_{sh} = 3Z\langle T_e\rangle + 2\langle T_i\rangle$

The sheath acceleration is proportional to the ionization state, i.e. the charge of an ion. Erosion is determined by the cumulative product of all ion fluxes and the corresponding sputter yields.

The effective perpendicular ion flux of a species i – compared to the hydrogen flux - is given by the concentration c_i (eq. 24).

(24) $\Gamma_{eff,i} = c_i \Gamma_{\perp,i},$

The angle of incidence after sheath acceleration was assumed to be normal, if $\rho_{gyro} \gg \lambda_D$ [18], or $\theta \approx 65°$ for shallow magnetic field angles of $\alpha \approx 5°$ [16]. In the latter case, the sheath is wide enough to force gyrating ions on curved trajectories during sheath acceleration. Sputter yields by impinging ions are calculated for each ion species with the corrected fit formula published by Eckstein [17].

2.3.5 Self-sputtering

The kinetic energy of each neutral W projectile is taken from its velocity vector in MC, yielding a sputter yield $\bar{Y}_{self}$, averaged over all simulated particles, assuming normal incidence.

(25) $Y_{ion,eff} = \sum_{i=ion\ species} c_i Y_i$

$\bar{Y}_{CXn}$ denotes the average effective sputter yields by neutrals obtained with CELLSOR. $Y_{ion,eff}$ (eq. 25, effective impurity ion sputtering) and $\bar{Y}_{CXn}$ (sputtering by neutrals) are normalized to the known fuel ion influx $\Gamma_\perp$. The prompt redeposition factor f_{dep} (eq. 22) is used to estimate the fraction of eroded material, that reimpinges to the wall immediately.

2.3.6 Net Mass Erosion / fpy

The net mass erosion in kg / fpy considering prompt redeposition and self-sputtering is computed by eq. 27. Eq. 26 connects the fraction of eroded material to the recycling flux (eq. 17) and gives the eroded W flux Γ_W.

(26) $\Gamma_W = (1 - f_{dep})(Y_{ion,eff} + \bar{Y}_{CXn})\Gamma_\perp$
(27) $\Delta M_{FW} = \Gamma_W \bar{Y}_{self} f_{dep} S_{FW} M_W t_{yr}$

S_{FW} is the FW area, t_{yr} a year in seconds and M_W the mass of a single tungsten ion.

3. Code Verification

A more detailed description of the numerics and computational mechanics of CELLSOR cannot be part of the scope of this paper. However, a verification of the mathematical correctness – within the given code assumptions – is presented by comparison calculations with the well-established and by far more complex and sophisticated MC code EIRENE [18]. Therefore, two reference cases with ITER- and DEMO-like parameters were computed (with a pure D plasma) with both codes for benchmark comparisons.

CELLSOR was computing with 1300 equidistant cells, whereas EIRENE was using a fixed resolution with 501 reference marker positions, which were not equidistant and prioritized in the plasma edge and SOL region. EIRENE – capable of simulating further reactions - was used "only" with reaction rate coefficients for the same reactions as CELLSOR (eq. 3-6). Reference parameters of both cases, which need to be equal for comparison, but not necessarily exact for ITER and DEMO, are shown in tab. 1.

Parameter	value (*DEMO* case)	value (*ITER* case)
$\bar{n}_0$ [$10^{20}\mathrm{m}^{-3}$]	1.2	1.2
$\langle T \rangle_0$ [keV]	24.9	10
α_n	0.5	0.3
α_T	1	0.5
$\bar{n}_{ped}$ [$10^{20}\mathrm{m}^{-3}$]	0.67	0.8
$\bar{n}_{sep}$ [$10^{20}\mathrm{m}^{-3}$]	0.2	0.35
$\langle T \rangle_{ped}$ [keV]	5.6	5
$\langle T \rangle_{sep}$ [keV]	0.2	0.2
Δ_{ped}	0.07	0.04
λ_n [m]	0.13	0.034
λ_T [m]	0.001	0.017
$\langle T \rangle_{min}$ [keV]	0.01	0.005
Δ_{SOL} [m]	0.2	0.1
a [m]	2.643	2
R [m]	9	6.2
$\Gamma_\perp$ [$10^{20}\mathrm{m}^{-2}\mathrm{s}^{-1}$]	10	1 (avg)
T_{wall} [K]	800	500
E_{D^+} [keV]	0.1	0.04

Tab. 1: Parameter for the *DEMO* [22, 23, 24, 25, 26] and *ITER* [6, 19, 20, 21] reference cases.

3.1. Radial Neutral Deuterium Density

The neutral particle density within each Monte Carlo cell at radial position ρ was computed within CELLSOR by weighted particle counting folded with the source strength, i.e. the recycling flux density.

(28) $n_n(\rho) = \frac{f_{rec}}{N} \sum w_i \frac{t_{dwell,i}}{V_{cell,i}}$

Fig. 1 shows the computed neutral density profile of the benchmark calculations between CELLSOR and EIRENE for the ITER-like and DEMO-like reference cases. The histograms show very good agreement, showing good statistics close to the wall in the SOL- and pedestal region, and large scattering close to the centre of the core plasma. Fig. 2 shows the region within 20 cm close to the first-wall, which yields the volumetric source strength S inside the SOL being plugged into the continuity equation (eq. 7).
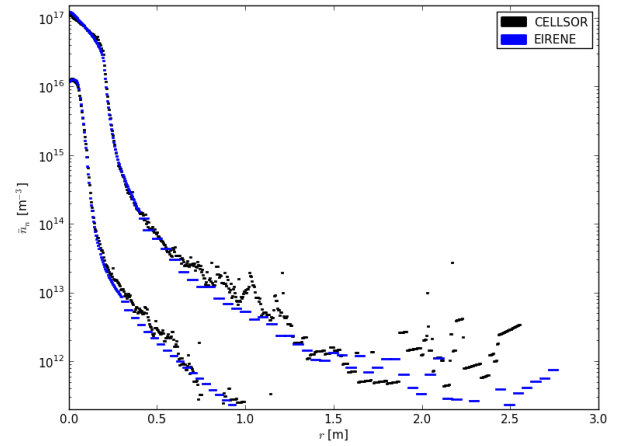

Fig. 1: comparison of the neutral density profiles computed by *CELLSOR* and *EIRENE* (upper histograms: DEMO-like case, lower histograms: ITER-like case).
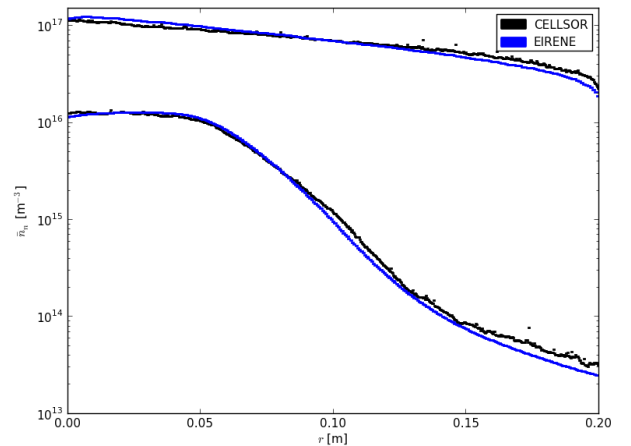

Fig. 2: comparison of the neutral density profiles computed by *CELLSOR* and *EIRENE* in the *SOL* region (DEMO case).

4. Parameter Studies
4.1. Bold SOL cases

The effects of SOL transport and density level on PWI in the main chamber, were studied systematically. Therefore, 6 distinguishable bold test cases were chosen (tab. 2), covering the range of observed SOL regimes, i.e. from

weak to strong diffusive transport up to a density shoulder formation case with strong convective transport. In the convective case, a very conservative equilibrium value was chosen (compared to experimentally observed intermittent blob frequencies and velocities). For DEMO, transport strength and upstream density were estimated in an expected range for detached divertor conditions and large power entering the SOL ($P_{SOL} > 240$ MW). The low density case is the absolutely optimistic lower upstream density limit to achieve divertor detachment, needing a radiated power fraction (SOL and divertor) of $f_{pow} > 0.95$ and momentum loss $f_{mom} = \frac{2}{3}$, assuming a conduction limited regime for parallel heat transport. The reference case represents a case of medium values for diffusive and convective transport strength, as well as upstream midplane separatrix density.

Test case	$D_\perp$ [m²/s]	$v_\perp$ [m/s]	n_{sep} [e^{20} m^{-3}]	$\Gamma_\perp$ ($\Delta_{SOL} = 0.1$ m) [10^{20} m$^{-2}s^{-1}$]
Reference	0.5	5	0.5	2.92
Weak transport	0.1	0.1	0.5	0.07
Strong transport	1	5	0.5	6.61
Low density	0.5	5	0.25	1.36
High density	0.5	5	1	6.75
Density shoulder	0.5	25	0.5	24.09

Tab. 2: Bold SOL physics cases distinguished by diffusive and convective radial transport strength and separatrix density.

All cases were computed with DEMO-like parameters similar to those listed in tab. 1, but with $n_{ped} = 10^{20}$ m^{-3} and - if not varied during the study - $\Delta_{SOL} = 15$ cm, using the calculated consistent values for $\Gamma_\perp$.

6.1.1 Neutral Damage

The scope of the first CELLSOR-study was to investigate the following question: how harmful are neutral particles (D, T), born by CX in a certain plasma region for the 6 defined bold test cases (tab. 2)? To answer this question, the cell positions of ultimate CXn, i.e. the spot of last recharge of neutrals before wall-impingement, were investigated for D- and T-neutrals.
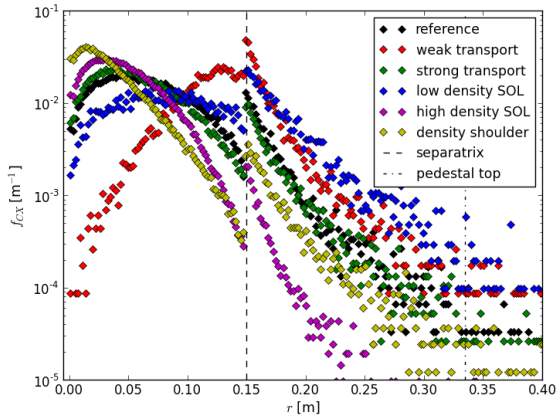

Fig. 3: probability distribution of ultimate recharges, i.e. total fraction per length $f_{CX} = p_{CX}/l$ ($\int f_{CX}dx = 1$).

Fig. 3 shows the spatial probability distribution of ultimate recharges, with the wall being located at $r = 0$ m. The distributions peak either in the far-SOL (density shoulder, high density, strong transport cases), or in the outer pedestal (weak transport, low density case). Clearly, a far-SOL buffer zone forms in high density and strong transport cases. Also, less than 10^{-3} of the wall-impinging neutrals come straight from the confined plasma region. A strong argument, that the large statistical noise of the histograms (fig. 1) around the plasma core, is acceptable for neutral particle PWI studies with CELLSOR. The number of simulated particles is up to 5 orders of magnitude greater within the region of interest (SOL, pedestal), compared to the plasma centre (fig. 1).

The spatial probabilities for ultimate CXn cannot be used to assess the actual harm potential of neutrals, as the plasma in the SOL was cold (10-200 eV) compared to the pedestal plasma (200-5600 eV). Therefore, multiplying f_{CX} with the actual sputter yield $Y(E, \theta)$, calculated for each particle at wall-impingement, translates the positional recharge analysis into a harm potential analysis, as the background ion temperature and impingement angles are added to the analysis.
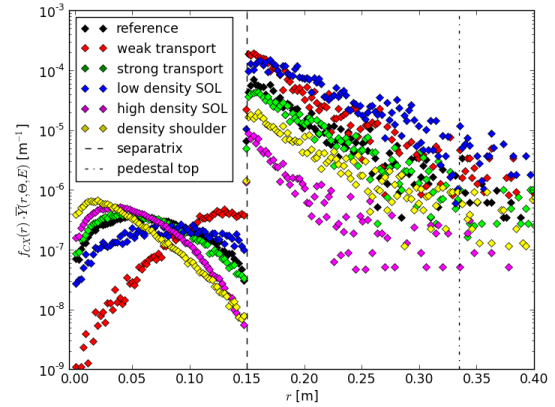

Fig. 4: average sputter yield of wall-impinging neutrals (D, T) weighted with the probability distribution of ultimate recharges.

Fig. 4 shows the average sputter yield of impinging particles born by CX in a cell at position r, multiplied with spatial probability f_{CX}. The relative sputter yield Y_{rel} of each case can be epressed as the area under a "curve" in fig. 4 (eq. 29).

$$(29) \quad Y_{rel} \equiv \int \bar{Y}_{CX}(r, \theta, E) f_{CX}dx$$

Clearly, the most harmful region lies within the pedestal, where the temperature gradient is steep (-34 keV/m). The separatrix and edge pedestal peaks are several hundred times more pronounced than before (fig. 3), i.e. particles are 100-fold less harmful being ultimately recharged within the cold SOL ($10 - 200$ eV).

High density cases, i.e. strong transport, density shoulder and high separatrix density cases, still show a buffer zone in the far-SOL and therefore a suppressed peak in the

outer pedestal, i.e. only in low density cases, hot particles from the pedestal will most likely impact the first-wall unimpeded.

The conclusion regarding the neutrals could be, that high density cases are favorable for DEMO from PWI point of view. This conclusion would be correct if the fluxes would be equal in each bold test case. For erosion however, the recycling flux, which is governed by the transport strength and density level, is decisive.
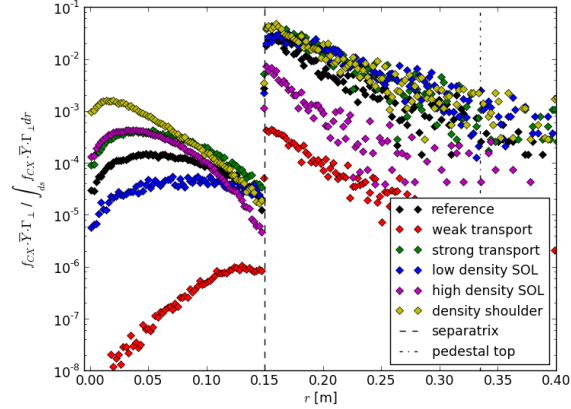

Fig. 5: Radially resolved sputter contribution $Y_{rel}\Gamma_\perp$ for the 6 bold test cases, normalized to density shoulder (ds) integral.

Consequently, the spatial sputter yield probabilities of fig.4 were multiplied with the consistent flux for each case (fig. 5) and normalized to the density shoulder case (ds), i.e. $\int_{ds} f_{CX}\overline{Y}\,\Gamma_\perp dx = 1$. Fig. 5 shows, that including the fluxes into the consideration, from PWI side ("area" under "curves"), low density and weak transport cases are by far (factor > 100) favorable to minimize the FW damage by CX neutrals. However, the core plasma performance and also divertor detachment in DEMO, will require high upstream densities.

Of course, the worst simulated case is the density shoulder case, being extremely conservative regarding the transport strength (especially the convective one). Other cases, with lower but equal transport strength, for instance the reference- and high density case, showed different pronounciations of the pedestal- and far-SOL peaks, but a similar curve-area, i.e. global damage by neutrals.

6.1.1.1   Pedestal Top Temperature

Fig. 6 shows the influence of the pedestal top temperature on the average sputter yield of wall impinging CX neutrals. The pedestal top temperature is foreseen to be at least 5.6 keV for DEMO [19]. In the unexpected regime of very low pedestal temperatures, the harm potential by CX neutrals was observed to be strongly reduced (factor $8-10$), whereas in the expected range of 4-8 keV, the effect was only minor (factor $1.7-1.8$). The role of the separatrix temperature (between 100-800 eV) was within a factor of 2 in the expected range ($\langle T\rangle_{ped} = 4-8$ keV).
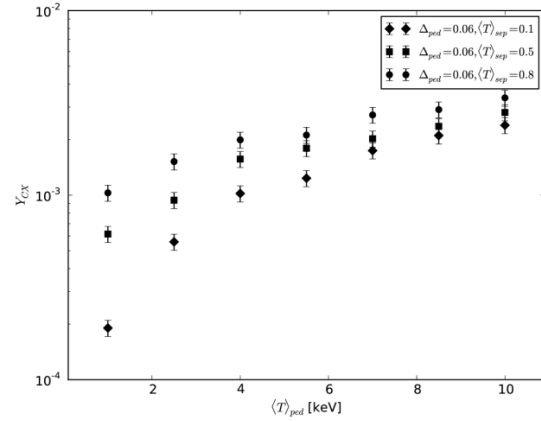

Fig. 6: Sputter Yield of wall impinging CX neutrals vs. pedestal top temperature for separatrix temperatures of 100 / 500 / 800 eV.

6.1.2   Net First-Wall Erosion Including Ion Damage, prompt redeposition and self-sputtering

Impurity i	c_i	$\langle Z_i\rangle$
N	0.02	7
He	0.05	2
W	$2\cdot 10^{-5}$	60

Tab. 3: Impurity mix with N as seeding gas, showing concentration c_i of species i and avg. charge state $\langle Z_i\rangle$.

The net global average damage of the main chamber FW is dominated by the impinging perpendicular flux. Due to the transport parallel to the magnetic field lines into the divertor, the gap size Δ_{SOL}, i.e. the distance between separatrix and wall, was identified as the most promising control parameter for wall protection. The PWI analysis was so far restricted to the damage by harmful CXn (D, T). In a last step, the analysis was completed by adding damage by impurity ions accelerated in the Debye Sheath (eq. 23), and prompt redeposition (eq. 20-22) and W self-sputtering (eq. 24-25), the global average net mass loss by erosion (eq. 26-27) was investigated as a function of the gap parameter Δ_{SOL} (fig. 7).
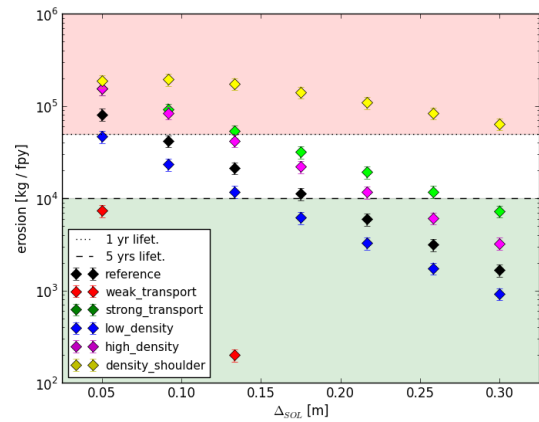

Fig. 7: Net mass erosion in kg / fpy by ions (D, T, He, N, W) and neutrals (D, T) for the bold SOL test cases (tab. 2)

Tab. 3 shows the impurity mix of the plasma. Within this analysis, N was chosen to be the one seeding gas species and a pure-W FW was assumed, i.e. no Fe content. Please note, that the ion damage analysis was not as deep as the neutral damage analysis. However, the charge states were estimated to be very high and also a normal angle of incidence was assumed for ions, i.e. a crude but conservative analysis.

Fig. 7 shows, that the flux effect is pronounced in weak transport cases and suppressed for strong convective transport (density shoulder case). The intermediate reference case indicates for DEMO, that an ITER-like gap size of $\Delta_{SOL} \approx 5$ cm would mean a net mass erosion of 80 t of W / fpy, which corresponds to a component lifetime of 0.68 fpys. Increasing the gap to $\Delta_{SOL} \approx 15$ cm would increase the lifetime τ_{FW} to about 4 fpys (factor of 5), which must be considered feasible for a FPP. Even $\Delta_{SOL} > 8$ cm could be regarded as minimum feasibility distance ($\tau_{FW} > 1$fpy), considering the strongly conservative assumptions leading to generally stronger erosion.

Comparison of the low- and high density case shows, that DEMO requires to be operated at

   a) sufficiently high upstream densities for divertor detachment and fusion performance,
   b) sufficiently low upstream densities regarding PWI aspects.

The net mass erosion in kg /fpy, grows almost perfectly anti-proportional to the upstream separatrix density, i.e. at $\Delta_{SOL} = 12.86$ cm, the net erosion is by a factor of 4 in favor of the lower density case compared to the high density case.

Summary & Conclusion

The fast 1.5d neutral particle MC code CELLSOR was developed to introduce PWI considerations into DEMO systems code studies. The code was successfully benchmarked against the well-established and more sophisticated code EIRENE (fig. 1-2). The code showed good statistics in the region of interest, i.e. the SOL and edge pedestal, and large scattering in the plasma core. Neutral particle studies showed (fig. 3-5), that harmful neutrals originate almost exclusively from the plasma region behind the separatrix ($>99.9\%$), which allows to regard CELLSOR as a feasible tool for simplified PWI studies.

All studies were performed with 6 bold test cases (tab. 2), distinguishing strong and weak diffusive and convective transport, and high and low upstream separatrix density levels. Even the low density case was chosen such, that simple 2-point model considerations would just allow detached divertor conditions, which are necessary for DEMO operation, however at a very optimistic radiated power fraction of $f_{pow} > 0.95$ in the SOL and divertor.

For neutrals, the high density cases showed a buffer zone formation in the far-SOL (fig. 5), taking up energy from CX neutrals, which were born in the hot pedestal regions, and thereby reducing the impingement energy at the FW. In such cases, a complete analysis should include the SOL power balance, which is foreseen to be incorporated in upcoming studies.

The particle flux to the wall, controllable by the gap size Δ_{SOL}, was identified to be the most dominant driver for FW erosion. The fluxes were drastically increased in high density and strong transport cases (fig. 5, fig. 7). Clearly, the buffer zone effect in high density cases is too weak, to make them favorable for DEMO from PWI point of view. However, for high machine performance, DEMO will most likely operate at high densities. Still, Δ_{SOL} was proven to be a good control parameter for FW protection (fig. 7) in most cases, affecting the perpendicular flux onto the FW, being most efficient for weak $D_\perp$ and $v_\perp$.

Considering N as impurity seeding species, a 5% He dilution of the plasma and a concentration of $2 \cdot 10^{-5}$ of W impurity, the global average equilibrium net mass loss by erosion, considered for neutrals and ions (incl. prompt redeposition and self-sputtering), was ≈ 16 t W / fpy at a gap width of $\Delta_{SOL} = 0.15$ m. The FW was considered to be coated with 2 mm of pure W, which gives a total mass of 54 t W. At an ITER-like gap-size ($\Delta_{SOL} = 5$ cm), the net erosion would be ≈ 80 t W / fpy, yielding a component lifetime of only 0.68 fpy, which is not tolerable for DEMO. The FW lifetime could be extended to 1 (5) fpy, by increasing the gap width to 8 (17) cm (reference case, conservative assumptions for ions).

The pedestal temperature studies showed, that around the expected value for DEMO of 5.6 keV, the CX neutral damage increases almost linearly by a factor of 1.7-1.8. This indicates a further issue, namely that the strong uncertainty in pedestal pressure and temperature scalings from nowadays machines to DEMO, results in uncertainties for assessment of the damage potential of DT-neutrals.

References

[1] ITER Physics Basis Editors and ITER Physics Expert Group Chairs and Co-Chairs and ITER Joint Central Team and Physics Integration Unit, Chapter 1: Overview and summary, *Nucl. Fus.* **39** (1999) 2137

[2] F. Romanelli et al., *Fusion Electricity - EFDA* (2012)

[3] G. Federici et al., *Fusion Eng. Des.* **89** (2014) 882–9

[4] M. Kovari et al., *Fusion Eng. Des.* **89** (2014) 3054-69

[5] C. Reux et al., *Nucl. Fus.* **55** (2015) 10pp

[6] V. Kotov et al., Phys. Scr. **T138** (2009) 4pp

[7] J.N. Brooks, *Fusion Eng.Des.***60** (2002) 515-526

[8] G. Fussmann et al., *Nucl. Fus. Res.* **2** (1994) 143-148

[9] D. Reiter, *Springer* (1987) The data file HYDHEL

[10] D. Reiter, *unpublished* (2015) The data file AMJUEL

[11] W. Eckstein, *IPP* **9/132** (2002)

[12] R. Dux, *IPP* **10/27** (2004)

[13] M. W. Thompson, *Philosophical Magazine* **18:152** (1968) 377-414

[14] L. Vainshteinet al., *J. Phys. B: At. Mol. Opt. Phys.* **44** (2011) 8pp

[15] P. Stangeby, *IOP Publishing Ltd.* (2000)

[16] P. Lindner et al., *ICPP & 25th EPS CCFPP* (1998)

[17] W. Eckstein, *Topics App. Physics* **110** (2007) 33-187

[18] D. Reiter, *unpublished* (2009) The EIRENE Code User Manual **11**

[19] A. Mekkaoui et al., *Contrib. Plasma Phys.* **54** (2014) 4-6

[20] ITER Technical Basis, *ITER EDA Documentazion Series* **24** (2002)

[21] E.M. Hollmann et al., *Nucl. Fus.* **52** (2012)

[22] T. Eich, *Nucl. Fus.* **53** (2013)

[23] L.J. Aubert et al., *Nucl. Fus.* **55** (2015)

[24] B. Lipschultz et al., *Plasma Science and Fusion Center* **02139** (2010)

[25] F. Militelloet al., *Plasma Phys. Control. Fusion* **55** (2013)

[26] H. Zohm, *Fusion Science and Technology* **58** (2010) 613-24